Featured in Physics

Exploring six modes of an optical parametric oscillator

Luis F. Muñoz-Martínez,[1,2] Felippe Alexandre Silva Barbosa,[3] Antônio Sales Coelho,[4,5] Luis Ortiz-Gutiérrez,[6] Marcelo Martinelli,[7,*] Paulo Nussenzveig,[7] and Alessandro S. Villar[8]

[1]*Departamento de Física, Universidade Federal de Pernambuco, 50670-901 Recife, Pernambuco, Brazil*
[2]*Departamento de Ciencias Básicas, Universidad del Sinú-Elías Bechara Zainúm, Cra 1w # 38-153, Montería, Córdoba, Colombia*
[3]*Instituto de Física Gleb Wataghin, Universidade Estadual de Campinas, 13083-859 Campinas, São Paulo, Brazil*
[4]*Departamento de Engenharia Mecânica, Universidade Federal do Piauí, 64049-550 Teresina, Piauí, Brazil*
[5]*Departamento de Engenharia, Centro Universitário UNINOVAFAPI, 64073-505 Teresina, Piauí, Brazil*
[6]*Instituto de Física de São Carlos, Universidade de São Paulo, P.O. Box 369, 13560-970 São Carlos, São Paulo, Brazil*
[7]*Instituto de Física, Universidade de São Paulo, P.O. Box 66318, 05315-970 São Paulo, Brazil*
[8]*American Physical Society, 1 Research Road, Ridge, New York 11961, USA*

(Received 6 March 2018; published 13 August 2018)

We measure the complete quantum state for six modes of the electromagnetic field produced by an optical parametric oscillator. The investigation involves the sidebands of the intense pump, signal, and idler fields generated by stimulated parametric down-conversion inside a triply resonant optical resonator. We develop a theoretical model to successfully interpret the experimental results. The model takes into account the coupling of the field modes to the phonon bath of the nonlinear crystal, clearly showing the roles of different physical effects in shaping the structure of the quantum correlations between the six optical modes.

DOI: 10.1103/PhysRevA.98.023823

I. INTRODUCTION

The optical parametric oscillator has been used since the early days of quantum optics to generate all sort of quantum states of light. The long list includes squeezed states [1], intense twin beams [2], Einstein-Podolsky-Rosen entangled states [3], the squeezed pump field [4], entangled beams [5], three-mode quantum correlations [6], and three-mode multicolor entanglement [7]. The field modes produced by the optical parametric oscillator contain intricate quantum properties that are not yet completely understood both in theory and in experiment.

The applications of these nonclassical states in the continuous-variable domain goes from the use of squeezing for ultrasensitive measurements [8,9] to the demands for entanglement in quantum information processing [10], with convergence of experiments for discrete and continuous variables of the electromagnetic field [11]. Moreover, multimode entangled states in the continuous-variable domain are interesting candidates for quantum information processing [12], leading to the search for sources involving modes defined in either time [13], frequency [14,15], or momentum [16].

The fundamental process for the generation of these nonclassical states of light is the reversible exchange of energy among the pump field and the two down-converted modes. With the aid of optical cavities, this effect is enhanced, and the output states can be calculated with the help of the input-output formalism for optical cavities and the master equation of the interacting Hamiltonian for the three modes of the field [17].

Nevertheless, a detailed investigation of the detection process leads to a more complete description of the quantum state represented in the basis of field quadratures [18]. In fact, optical detection is generally based on interferometric techniques, either by optical homodyning or by resonator self-homodyning [19]. On the other hand, the measured quantum noise of light is analyzed in the frequency domain with the help of an electronic local oscillator to filter the contribution at a given frequency, associated with the sidebands of the optical field. Therefore, with careful data treatment, it can be shown that although the three-mode description remains a valid approach, a more complete one can be obtained for the six detected modes of the field.

Our interest here is to present an explicit evaluation of the quantum state for the six sideband modes of the optical parametric oscillator (OPO) that are measured by homodyne techniques and to access modal correlations that would not be available in the simplified three-mode picture of single-beam quantum fluctuations (pump, signal, and idler). By explicitly using frequency modes of the field in the Hamiltonian, we are able to deal with open cavities, looking for a more faithful description of optical setups usually involved in the nonclassical state generation. This six-mode description allows the complete analysis of entanglement in the OPO, demonstrating a deep hexapartite entangled structure for this system. Moreover, the detailed sideband description puts in evidence the role of each field in the evolution of the system, something that remained implicit in the usual treatment [17]. This allows the complete analysis of the hexapartite entanglement, which will be treated in detail in another publication [20].

We begin by presenting the Hamiltonian for the sideband coupling in the nonlinear medium (Sec. II) and the evolution of the field operators under propagation on this medium (Sec. III). It is followed by the detailed model for the open cavity that is used to evaluate the operators of the output field (Sec. IV). With the relation between the output and the input modes, momenta of any order can be evaluated. In the present scenario,

*mmartine@if.usp.br

we will limit the study to the second-order momenta and the reconstruction of the covariance matrix (Sec. V). Nevertheless, the description would not be complete without the coupling of phonons to the sideband modes, included in the Hamiltonian of the system (Sec. VI). The obtained results are used to describe the latest experimental results from our setup at different pump powers (Sec. VII), with pump powers up to 75% above the oscillation threshold. The complete description of the OPO in terms of the measured sidebands opens the possibility to analyze the multipartite entanglement present in this system in a wide range of operational conditions (Sec. VIII).

II. INTERACTION HAMILTONIAN IN THE SIDEBANDS

Each annihilation operator of the field $\hat{a}^{(n)}(t)$ is associated with the electric field operator of a propagating wave and, in the limit of a cavity of infinite size, can be described by the contribution of operators at each frequency mode as [21]

$$\hat{a}^{(n)}(t) = e^{-i\omega_n t}\int_{-\omega_n}^{\infty} d\Omega e^{-i\Omega t}\hat{a}^{(n)}_{\omega_n+\Omega}, \tag{1}$$

where $\hat{a}_{\omega_n+\Omega}$ is the photon annihilation operator in the mode with frequency $\omega = \omega_n + \Omega$ and we explicitly identify the carrier frequency of each field ω_n and the frequency shift of each sideband relative to this carrier Ω. The mode n specifies different directions of propagation, polarizations, or carrier frequencies.

A common treatment in optical systems considers as the *carrier* the mode with a significant population of photons, which is much larger than the average number of photons in all other modes. Therefore, in a linearized description of the fields by their mean value and a fluctuation, where each mode is described as $\hat{a}^{(n)}_{\omega_n+\Omega} = \langle\hat{a}^{(n)}_{\omega_n+\Omega}\rangle + \delta\hat{a}^{(n)}_{\omega_n+\Omega}$, we consider that $|\alpha_{\omega_n}|^2 \equiv \langle\hat{a}^{(n)\dagger}_{\omega_n}\hat{a}^{(n)}_{\omega_n}\rangle \gg \langle\hat{a}^{(n)\dagger}_{\omega_n+\Omega}\hat{a}^{(n)}_{\omega_n+\Omega}\rangle$ for $|\Omega| > \epsilon$, where α_{ω_n} is the mean field of the carrier mode n and ϵ is the carrier linewidth.

We can describe the interaction among the fields in a medium with a second-order susceptibility χ with the help of an effective Hamiltonian

$$\hat{H}_\chi = i\hbar\frac{\chi}{\tau}[\hat{a}^{(0)}(t)\hat{a}^{(1)\dagger}(t)\hat{a}^{(2)\dagger}(t) - \text{H.c.}], \tag{2}$$

where τ is the time of flight through the medium and field indices 0, 1, and 2 stand for pump, signal, and idler modes, respectively.

Using linearization, we can rewrite this interaction Hamiltonian separating the contribution of each carrier and each sideband. In the triple product, only the terms satisfying the energy-conservation condition will prevail under propagation. This includes the relation for the carriers ($\omega_0 = \omega_1 + \omega_2$), as well as their sidebands.

This procedure will help to discriminate different contributions to the resulting Hamiltonian that come from each mode involved. We will have the triple product of the carriers, associated with the mean value of the intense fields, as a constant value that can be disregarded for the evolution of operators. Next, there will be a combination of bilinear Hamiltonians for the specific sidebands shifted by $\pm\Omega$ from the central carriers

$$\begin{aligned}\hat{H}_\chi(\Omega) = -i\hbar\frac{\chi}{\tau}\big[&\alpha^*_{\omega_0}\big(\hat{a}^{(1)}_{\omega_1+\Omega}\hat{a}^{(2)}_{\omega_2-\Omega} + \hat{a}^{(1)}_{\omega_1-\Omega}\hat{a}^{(2)}_{\omega_2+\Omega}\big)\\ &+\alpha_{\omega_1}\big(\hat{a}^{(0)\dagger}_{\omega_0+\Omega}\hat{a}^{(2)}_{\omega_2+\Omega} + \hat{a}^{(0)\dagger}_{\omega_0-\Omega}\hat{a}^{(2)}_{\omega_2-\Omega}\big)\\ &+\alpha_{\omega_2}\big(\hat{a}^{(0)\dagger}_{\omega_0+\Omega}\hat{a}^{(1)}_{\omega_1+\Omega} + \hat{a}^{(0)\dagger}_{\omega_0-\Omega}\hat{a}^{(1)}_{\omega_1-\Omega}\big) - \text{H.c.}\big],\end{aligned} \tag{3}$$

defined for $\Omega > \epsilon$ for convenience. Linear terms in the fluctuations will not satisfy energy conservation, and the contribution of trilinear or cubic terms will be negligibly small in comparison with the bilinear terms involving the intense mean fields of the carriers and will be disregarded in the present treatment. The Hamiltonian in Eq. (2) may be described by the sum over the contribution of each Hamiltonian from Eq. (3) for different frequencies Ω, $\hat{H}_\chi = \int_\epsilon^\infty \hat{H}_\chi(\Omega)\,d\Omega$. Therefore, under the validity of linearization, each set of sideband pairs defined by $\Omega > \epsilon$ is decoupled from other sets defined by $\Omega' \neq \Omega$.

On the other hand, upper and lower sidebands are coupled in pairs in Eq. (3). The field operators of these sidebands are pairwise measured by the treatment of detected photocurrents in the frequency domain [18,19]. The treatment for the evolution of these operators can be simplified if we change to the measurement basis involving symmetric ($\mathcal{S}$) and antisymmetric ($\mathcal{A}$) combinations of upper and lower sideband operators [18]:

$$\hat{a}^{(n)}_{s(a)} = \frac{1}{\sqrt{2}}\big[\hat{a}^{(n)}_{\omega_n+\Omega} \pm \hat{a}^{(n)}_{\omega_n-\Omega}\big]. \tag{4}$$

On this basis, the Hamiltonian given in Eq. (3) is rewritten as

$$\hat{H}_\chi(\Omega) = \hat{H}_{\chi s} + \hat{H}_{\chi a}, \tag{5}$$

where

$$\begin{aligned}\hat{H}_{\chi s(a)} = -i\hbar\frac{\chi}{\tau}\big[&\pm\alpha^*_{\omega_0}\hat{a}^{(1)}_{s(a)}\hat{a}^{(2)}_{s(a)} + \alpha_{\omega_1}\hat{a}^{(0)\dagger}_{s(a)}\hat{a}^{(2)}_{s(a)}\\ &+\alpha_{\omega_2}\hat{a}^{(0)\dagger}_{s(a)}\hat{a}^{(1)}_{s(a)} - \text{H.c.}\big],\end{aligned} \tag{6}$$

where the $+$ ($-$) sign is used for the symmetric (antisymmetric) combination of sidebands throughout this article. This Hamiltonian describes a process leading to two-mode squeezing involving down-converted modes $\hat{a}^{(1)}_{s(a)}$ and $\hat{a}^{(2)}_{s(a)}$ mediated by the intense pump field and two beam-splitter processes exchanging photons between the pump and each down-converted mode, mediated by the intense complementary down-converted field. These three processes lead to a rich entanglement dynamics that was understood as a source of tripartite entangled fields in the symmetric mode description [22]. Beyond this three-mode description, a rich mesh of entanglement dynamics involving six modes is generated by Eq. (3), combining creation and annihilation of pairs of photons in down-converted sidebands and photon exchange between pump and down-converted sidebands, leading to hexapartite entanglement among the involved modes [20].

On the other hand, Eq. (6) shows that the subspaces of symmetric and antisymmetric combinations of sidebands are not coupled by the nonlinear medium. Nevertheless, these correlations were already observed in experiments [18], and their origin is found somewhere else in the OPO, as we will see in Sec. IV.

III. EQUATIONS OF MOTION AND SOLUTION BY THE MATRIX METHOD

After passing through the nonlinear medium, the modes in subspaces of $\mathcal{S}$-$\mathcal{A}$ combinations of sidebands will interact according to the Hamiltonian given by Eq. (5). Therefore, the equations describing the evolution of the operators during their propagation through the medium are given by

$$\frac{d\hat{a}^{(0)}_{s(a)}}{d\xi} = -\chi\left[\alpha_{\omega_1}\hat{a}^{(2)}_{s(a)} + \alpha_{\omega_2}\hat{a}^{(1)}_{s(a)}\right], \tag{7}$$

$$\frac{d\hat{a}^{(1)}_{s(a)}}{d\xi} = \chi\left[\pm\alpha_{\omega_0}\hat{a}^{(2)\dagger}_{s(a)} + \alpha^{*}_{\omega_2}\hat{a}^{(0)}_{s(a)}\right], \tag{8}$$

$$\frac{d\hat{a}^{(2)}_{s(a)}}{d\xi} = \chi\left[\pm\alpha_{\omega_0}\hat{a}^{(1)\dagger}_{s(a)} + \alpha^{*}_{\omega_1}\hat{a}^{(0)}_{s(a)}\right], \tag{9}$$

where ξ is the normalized time evolution given by $\xi = t/\tau$.

Defining $\vec{\mathbf{A}}_{s(a)} = (\hat{a}^{(0)}_{s(a)}\hat{a}^{(0)\dagger}_{s(a)}\hat{a}^{(1)}_{s(a)}\hat{a}^{(1)\dagger}_{s(a)}\hat{a}^{(2)}_{s(a)}\hat{a}^{(2)\dagger}_{s(a)})^{T}$, the set of differential equations given by Eqs. (7)–(9) and their Hermitian adjoints can be written as

$$\frac{d\vec{\mathbf{A}}_{s(a)}}{d\xi} = \mathbf{M}_{\chi s(a)}\vec{\mathbf{A}}_{s(a)}, \tag{10}$$

where

$$\mathbf{M}_{\chi s(a)} = \chi\begin{pmatrix} 0 & 0 & -\alpha_{\omega_2} & 0 & -\alpha_{\omega_1} & 0 \\ 0 & 0 & 0 & -\alpha^{*}_{\omega_2} & 0 & -\alpha^{*}_{\omega_1} \\ \alpha^{*}_{\omega_2} & 0 & 0 & 0 & 0 & \pm\alpha_{\omega_0} \\ 0 & \alpha_{\omega_2} & 0 & 0 & \pm\alpha^{*}_{\omega_0} & 0 \\ \alpha^{*}_{\omega_1} & 0 & 0 & \pm\alpha_{\omega_0} & 0 & 0 \\ 0 & \alpha_{\omega_1} & \pm\alpha^{*}_{\omega_0} & 0 & 0 & 0 \end{pmatrix}.$$

From Eq. (10) the field leaving the crystal can be written as

$$\vec{\mathbf{A}}_{s(a)}|_{\xi=1} = \mathbf{G}_{s(a)}(\chi)\vec{\mathbf{A}}_{s(a)}|_{\xi=0}, \tag{11}$$

where

$$\mathbf{G}_{s(a)}(\chi) = \exp\left(\int_0^1 d\xi \mathbf{M}_{\chi s(a)}\right). \tag{12}$$

The matrix $\mathbf{G}_{s(a)}(\chi)$ is defined as the *gain matrix of the medium* and allows the evaluation of all $\hat{a}^{(n)}_{\omega_n\pm\Omega}$ and their Hermitian adjoints after passing through the crystal.

In the calculation of the evolution of the terms inside the cavity, it will be useful to play with all creation and annihilation operators of the involved sidebands in the vector form $\vec{\mathbf{A}} = (\hat{a}^{(0)}_{\omega_0+\Omega}\hat{a}^{(0)\dagger}_{\omega_0+\Omega}\cdots\hat{a}^{(0)}_{\omega_0-\Omega}\hat{a}^{(0)\dagger}_{\omega_0-\Omega}\cdots)^{T}$, related to vectors $\vec{\mathbf{A}}_{s(a)}$ as

$$\vec{\mathbf{A}} = \mathbf{\Lambda}(\vec{\mathbf{A}}_s, \vec{\mathbf{A}}_a)^{T}, \tag{13}$$

where the transformation matrix has the form

$$\mathbf{\Lambda} = \mathbf{\Lambda}^{-1} = \frac{1}{\sqrt{2}}\begin{pmatrix} \mathbf{1}_{6\times6} & \mathbf{1}_{6\times6} \\ \mathbf{1}_{6\times6} & -\mathbf{1}_{6\times6} \end{pmatrix}, \tag{14}$$

where $\mathbf{1}_{6\times6}$ are identity matrices of order 6. Taking into account Eqs. (11) and (13), the transformation of the field operators that propagated through the medium is given by

$$\vec{\mathbf{A}}|_{\xi=1} = \mathbf{G}(\chi)\vec{\mathbf{A}}|_{\xi=0}, \tag{15}$$

where

$$\mathbf{G}(\chi) = \mathbf{\Lambda}(\mathbf{G}_s(\chi) \oplus \mathbf{G}_a(\chi))\mathbf{\Lambda}. \tag{16}$$

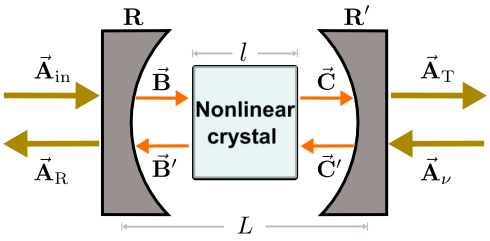

FIG. 1. Basic configuration of OPO, consisting of a nonlinear medium of length l inside a linear cavity of length L, made of one coupling mirror (left) and one end mirror (right) accounting for spurious losses.

The symbol $\oplus$ represents a direct sum, resulting in a block-diagonal matrix.

Thanks to the bilinear form of the Hamiltonian in Eq. (3), we have a linear evolution of the coupling of different fields through the medium, which will contribute to the equations describing their evolution inside a cavity.

IV. PHYSICAL EFFECT OF THE OPTICAL CAVITY

It must be kept in mind that our goal is to theoretically model the evolution of the sideband modes of an OPO, consisting of a nonlinear crystal located in a linear cavity that we assume has arbitrary losses for the fields involved, as described in Fig. 1. The coupling mirror has reflection and transmission coefficients, r_n and t_n, for each carrier, and the end mirror, with reflection coefficient r'_n and transmission coefficient t'_n, accounts for spurious losses (which may include absorption in the crystal or scattering on the optical interfaces). These coefficients can be conveniently described by loss parameters γ_n and γ'_n as

$$r_n = e^{-\gamma_n}, \quad t_n = \left(1 - r_n'^{2}\right)^{1/2},$$
$$r'_n = e^{-\gamma'_n}, \quad t'_n = \left(1 - r_n'^{2}\right)^{1/2}. \tag{17}$$

The total loss in a round trip can be directly evaluated from $\gamma^t_n = \gamma_n + \gamma'_n$.

The equations relating each field operator inside and outside the cavity (Fig. 1) are given by the beam-splitter transformation

$$\vec{\mathbf{A}}_{\rm R} = \mathbf{R}\vec{\mathbf{A}}_{\rm in} + \mathbf{T}\vec{\mathbf{B}}', \quad \vec{\mathbf{B}} = \mathbf{T}\vec{\mathbf{A}}_{\rm in} - \mathbf{R}\vec{\mathbf{B}}', \tag{18}$$

$$\vec{\mathbf{A}}_{\rm T} = \mathbf{R}'\vec{\mathbf{A}}_{\nu} + \mathbf{T}'\vec{\mathbf{C}}, \quad \vec{\mathbf{C}}' = \mathbf{T}'\vec{\mathbf{A}}_{\nu} - \mathbf{R}'\vec{\mathbf{C}}, \tag{19}$$

with

$$\mathbf{R} = \mathrm{diag}(r_0 r_0 r_1 r_1 r_2 r_2 r_0 r_0 \cdots),$$
$$\mathbf{T} = \mathrm{diag}(t_0 t_0 t_1 t_1 t_2 t_2 t_0 t_0 \cdots),$$
$$\mathbf{R}' = \mathrm{diag}(r'_0 r'_0 r'_1 r'_1 r'_2 r'_2 r'_0 r'_0 \cdots),$$
$$\mathbf{T}' = \mathrm{diag}(t'_0 t'_0 t'_1 t'_1 t'_2 t'_2 t'_0 t'_0 \cdots), \tag{20}$$

keeping the vector ordering for the field operators we used in the previous section. The fields described by $\vec{\mathbf{A}}_{\rm in}$ enter the cavity through the coupling mirror, while $\vec{\mathbf{A}}_{\nu}$ models the fields associated with vacuum modes coupled through spurious losses.

Each field $\hat{a}^{(n)}_{\omega_n\pm\Omega}$ will be transformed by the gain inside the crystal as described by Eq. (15). In addition, their phase will evolve during the propagation along the cavity. Under perfect phase-matching conditions [23], if the refractive index for the fields is close enough, we may consider that the evolution of the phase commutes with the gain. Therefore, the relation between the propagating fields on each side of the cavity will be given by

$$\vec{\mathbf{C}} = e^{-i\boldsymbol{\varphi}}\mathbf{G}(\chi)\vec{\mathbf{B}}, \quad \vec{\mathbf{B}}' = e^{-i\boldsymbol{\varphi}}\mathbf{G}(\chi)\vec{\mathbf{C}}'. \tag{21}$$

The phase vector

$$\boldsymbol{\varphi} = \boldsymbol{\varphi}(\Omega) \oplus \boldsymbol{\varphi}(-\Omega), \tag{22}$$

with

$$\boldsymbol{\varphi}(\Omega) = \mathrm{diag}\big(\varphi^{(0)}_{\Omega}, -\varphi^{(0)}_{\Omega}\varphi^{(1)}_{\Omega}, -\varphi^{(1)}_{\Omega}, \varphi^{(2)}_{\Omega} - \varphi^{(2)}_{\Omega}\big),$$

gives a different contribution for each sideband depending on the frequency shift Ω and on the carrier frequency ω_n,

$$\boldsymbol{\varphi}^{(n)}_{\Omega} = \frac{\omega_n + \Omega}{2\,\Delta f_n}, \tag{23}$$

where $\Delta f_n = c/2L^{(n)}_{\mathrm{op}}$ is the free spectral range for mode n, with $L^{(n)}_{\mathrm{op}} = L + l(\mathfrak{n}_n - 1)$ being the effective optical length between the cavity mirrors, depending on the crystal refractive index $\mathfrak{n}_n$ and on the speed of light c. Evidently, the effective phase contribution will depend on the detuning between the carrier and the nearest cavity mode ω^c_n, an integer multiple of $2\pi\,\Delta f_n$, given by $\Delta_n = \omega_n - \omega^c_n$.

An important point related to the evolution of the sidebands should be noted. Each operator will undergo a different phase evolution, depending on its frequency. That will mix symmetric and antisymmetric modes, even for null carrier detuning, since upper and lower sidebands will, in this case, undergo opposite phase evolutions. This is the cause of the correlations between symmetric and antisymmetric modes observed in [18].

Combining beam-splitter transformation, phase evolution, and gain, expressed in Eqs. (18)–(21), we can derive a linear transformation for the reflected modes, coupled to the incident modes on the OPO, as

$$\vec{\mathbf{A}}_{\mathrm{R}} = \mathbf{R}_{\chi}\vec{\mathbf{A}}_{\mathrm{in}} + \mathbf{T}'_{\chi}\vec{\mathbf{A}}_{\nu}, \tag{24}$$

where

$$\mathbf{R}_{\chi} = \mathbf{R} - \mathbf{T}e^{-i\boldsymbol{\varphi}}\mathbf{G}(\chi)\mathbf{R}'e^{-i\boldsymbol{\varphi}}\mathbf{G}(\chi)\mathbf{D}(\chi)\mathbf{T}, \tag{25}$$

$$\mathbf{T}'_{\chi} = \mathbf{T}e^{-i\boldsymbol{\varphi}}\mathbf{G}(\chi)[\mathbf{I} + \mathbf{R}'e^{-i\boldsymbol{\varphi}}\mathbf{G}(\chi)\mathbf{D}(\chi)\mathbf{R}e^{-i\boldsymbol{\varphi}}\mathbf{G}(\chi)]\mathbf{T}', \tag{26}$$

and

$$\mathbf{D}(\chi) = [\mathbf{1} - \mathbf{R}e^{-i\boldsymbol{\varphi}}\mathbf{G}(\chi)\mathbf{R}'e^{-i\boldsymbol{\varphi}}\mathbf{G}(\chi)]^{-1}. \tag{27}$$

We should note that the conversion matrix given by Eq. (14), relating individual modes to the symmetric-antisymmetric combination, commutes with the reflection and transmission matrices given by Eq. (20) but not with the phase-evolution matrix. This is consistent with the fact that the coupling of symmetric and antisymmetric modes comes from the opposite phase evolution for the sidebands. Another interesting point of the formalism adopted here is that it allows the evaluation of the complete covariance matrix for the sideband modes in an approach valid for lossy cavities beyond the narrow-band regime employed in Ref. [24]. In the extreme limit, it could be used to study the transformation of field in doubly resonant cavities, even for the mode undergoing a single pass through the nonlinear medium.

V. HEXAPARTITE QUANTUM STATE

In a way consistent with the description used in Ref. [18], we can evaluate the covariance matrix for the field quadratures $\hat{p}^{(n)}_{\omega}$ and $\hat{q}^{(n)}_{\omega}$ related to the photon annihilation $\hat{a}^{(n)}_{\omega}$ operator as $\hat{a}^{(n)}_{\omega} = (\hat{p}^{(n)}_{\omega} + i\hat{q}^{(n)}_{\omega})/2$, satisfying the commutation relation $[\hat{p}^{(n)}_{\omega}, \hat{q}^{(n)}_{\omega'}] = 2i\delta(\omega - \omega')$. The relevant quadrature operators can be ordered in a column vector $\vec{\mathbf{X}} = (\hat{p}^{(0)}_{\omega}\hat{q}^{(0)}_{\omega}\cdots\hat{p}^{(n)}_{\omega'}\hat{q}^{(n)}_{\omega'}\cdots)^T$, which is directly related to the vector of field operators by $\vec{\mathbf{X}} = \mathbf{N}\vec{\mathbf{A}}$.

Second-order momenta of the field operators are all contained in the symmetrized covariance matrix, evaluated over the quantum state of the system as

$$\mathbf{V} = \tfrac{1}{2}(\langle\vec{\mathbf{X}}\cdot\vec{\mathbf{X}}^T\rangle + \langle\vec{\mathbf{X}}\cdot\vec{\mathbf{X}}^T\rangle^T). \tag{28}$$

Diagonal elements of $\mathbf{V}$ represent variances of single-mode quadrature operators, denoted as, e.g., $\Delta^2\hat{p}^{(n)}_{\omega} \equiv \langle\hat{p}^{(n)}_{\omega}\hat{p}^{(n)}_{\omega}\rangle$. Off-diagonal elements are correlations between different quadratures operators, such as in, e.g., $C(\hat{p}^{(n)}_{\omega}\hat{p}^{(m)}_{\omega'}) \equiv (\langle\hat{p}^{(n)}_{\omega}\hat{p}^{(m)}_{\omega'}\rangle + \langle\hat{p}^{(m)}_{\omega'}\hat{p}^{(n)}_{\omega}\rangle)/2$.

The basis transformation given by matrix $\mathbf{N}$ applied to Eq. (24) results in quadrature operators $\vec{\mathbf{X}}_{\mathrm{R}} = \widetilde{\mathbf{R}}_{\chi}\vec{\mathbf{X}}_{\mathrm{in}} + \widetilde{\mathbf{T}}'_{\chi}\vec{\mathbf{X}}_{\nu}$, where $\widetilde{\mathbf{R}}_{\chi} = \mathbf{N}\mathbf{R}_{\chi}\mathbf{N}^{-1}$, $\widetilde{\mathbf{T}}'_{\chi} = \mathbf{N}\mathbf{T}'_{\chi}\mathbf{N}^{-1}$. Thus, the evaluation of the covariance matrix for the output fields results in

$$\mathbf{V}_{\mathrm{R}} = \widetilde{\mathbf{R}}_{\chi}\mathbf{V}_{\mathrm{in}}\widetilde{\mathbf{R}}^T_{\chi} + \widetilde{\mathbf{T}}'_{\chi}\mathbf{V}_{\nu}\widetilde{\mathbf{T}}'^T_{\chi}, \tag{29}$$

where $\mathbf{V}_{\mathrm{in}}$ is the input field covariance matrix and $\mathbf{V}_{\nu}$ is the covariance matrix of the field entering through the cavity loss channels. For losses coupling the cavity to vacuum modes we have $\mathbf{V}_{\nu} = \mathbf{1}$.

The covariance matrix in the basis of $\mathcal{S}$-$\mathcal{A}$ combinations of sidebands will have the same form described in Ref. [18],

$$\mathbf{V}_{\mathrm{R}(s/a)} = \begin{pmatrix} \mathbf{V}_s & \mathbf{C}_{s/a} \\ (\mathbf{C}_{s/a})^T & \mathbf{V}_a \end{pmatrix}. \tag{30}$$

It is important to note that the elements in the covariance matrices $\mathbf{V}_s$ and $\mathbf{V}_a$ are related by a $\pi/2$ rotation on the quadrature phase space, changing $\hat{p}_s \to \hat{q}_a$ and $\hat{q}_s \to -\hat{p}_a$ in covariance terms [e.g., $C(\hat{p}^{(n)}_s\hat{q}^{(m)}_s) = -C(\hat{q}^{(n)}_a\hat{p}^{(m)}_a)$, $\Delta^2\hat{p}^{(n)}_s = \Delta^2\hat{q}^{(n)}_a$, etc.]. Therefore, the modeling described here is equivalent to the semiclassical approach often used in evaluation of the noise spectra with the help of Langevin equations [18,21,24,25], and both methods can be used to obtain the same amount of information about the $2n$ modes of sidebands for n modes of carriers. However, it is important to clarify that the method developed here is explicit in presenting the physical origin of the correlations between symmetric and antisymmetric modes, something that was elusive in the semiclassical model. As demonstrated in Secs. II and IV, these correlations are not generated only by the cavity or by the squeezing generating term in Eq. (6), which is the only remaining term for operation below the oscillation threshold. It is their combination with

the beam-splitting term, associated with signal and idler mean fields, that will lead to these correlations.

Considering the particular case where the input is also a coherent state ($\mathbf{V}_{\text{in}} = \mathbf{1}$), for exact resonance of the carriers ($\Delta_n = 0$), we have

$$\mathbf{V}_s = \begin{pmatrix} \rho^{(0)} & 0 & \mu^{(01)} & 0 & \mu^{(02)} & 0 \\ 0 & \beta^{(0)} & 0 & \nu^{(01)} & 0 & \nu^{(02)} \\ \mu^{(01)} & 0 & \rho^{(1)} & 0 & \zeta^{(12)} & 0 \\ 0 & \nu^{(01)} & 0 & \beta^{(1)} & 0 & \epsilon^{(12)} \\ \mu^{(02)} & 0 & \zeta^{(12)} & 0 & \rho^{(2)} & 0 \\ 0 & \nu^{(02)} & 0 & \epsilon^{(12)} & 0 & \beta^{(2)} \end{pmatrix}, \quad (31)$$

with 12 independent terms, and

$$\mathbf{C}_{s/a} = \begin{pmatrix} 0 & 0 & 0 & -\kappa^{(01)} & 0 & -\kappa^{(02)} \\ 0 & 0 & \lambda^{(01)} & 0 & \lambda^{(02)} & 0 \\ 0 & \kappa^{(01)} & 0 & 0 & 0 & -\varrho^{(12)} \\ -\lambda^{(01)} & 0 & 0 & 0 & \eta^{(12)} & 0 \\ 0 & \kappa^{(02)} & 0 & \varrho^{(12)} & 0 & 0 \\ -\lambda^{(02)} & 0 & -\eta^{(12)} & 0 & 0 & 0 \end{pmatrix}, \quad (32)$$

with 6 independent terms.

Evaluation of the covariance matrix depends on the value of the mean fields, as can be seen in Eq. (11). If we go beyond the linearized model presented in Ref. [23], the contributions to the gain matrix can be explicitly scaled to the oscillation threshold $|\alpha^{\text{in}}_{\omega_0}|^2_{\text{th}}$ as

$$\chi^2 |\alpha_{\omega_0}|^2 = \frac{(1 - e^{-2\gamma_0})}{(1 - e^{-\gamma' _0})^2} \chi^2 |\alpha^{\text{in}}_{\omega_0}|^2_{\text{th}},$$

$$\chi^2 |\alpha_{\omega_j}|^2 = \frac{e^{2\gamma' _0}(1 - e^{-2\gamma_0})(\sqrt{\sigma} - 1)}{(e^{\gamma' _0} - 1)(e^{\gamma' _j} - 1)} \chi^2 |\alpha^{\text{in}}_{\omega_0}|^2_{\text{th}},$$

with $j = 1,2$, where the normalized pump power is given by $\sigma = |\alpha^{\text{in}}_{\omega_0}|^2 / |\alpha^{\text{in}}_{\omega_0}|^2_{\text{th}}$. Moreover,

$$\chi^2 |\alpha^{\text{in}}_{\omega_0}|^2_{\text{th}} = \frac{\left(1 - e^{-\gamma' _0}\right)^2 \left(e^{\gamma' _1} - 1\right)\left(e^{\gamma' _2} - 1\right)}{4(1 - e^{-2\gamma_0})}$$

implies that all the mean values can be related only to the cavity coupling terms and the normalized pump power.

We have retained here the consideration that evolution of the mean-field amplitude inside the crystal is negligible, as done in Ref. [23]. Further development can be done if we consider that these fields vary along the crystal. Nevertheless, in the integration in Eq. (12), we see that their evolution will not affect the linearity of the solution regarding the mode operators, and an effective contribution can be evaluated to obtain a precise description of the resulting covariances.

While this treatment could account for the OPO spectra above the threshold, it does not account for extra noise sources, such as the phonon-photon coupling in the crystal [25]. Its effect can be included in the interaction Hamiltonian, as we will see next. This extra phonon noise may also introduce correlations between $\hat{p}$ and $\hat{q}$ quadratures within $\mathbf{V}_{s(a)}$ matrices, as well as correlations in the $\mathbf{C}_{s/a}$ matrix, that can also be found in the case of nonzero cavity detunings.

VI. PHYSICAL EFFECT OF PHONONS IN THE NONLINEAR CRYSTAL IN THE QUANTUM NOISE OF LIGHT

In many experiments with above-threshold OPOs, an extra phase noise appears in the optical fields which is caused by the scattering of light by thermal phonons within the crystal and which considerably modifies the quantum state of the system. A detailed semiclassical analysis of this effect was realized in Ref. [25]. In this section we are going to establish a quantum model for this excess phase noise in order to have a consistent and complete quantum description of an OPO operating above threshold.

A. Complete interaction Hamiltonian

Photons that circulate inside the optical cavity of an OPO may eventually exert low radiation pressure on the crystal, leading to local-density fluctuations associated with acoustic phonons. On the other hand, fluctuations of the refractive index, of optical or mechanical origin, will result in small phase fluctuations, leading to Stokes and Brillouin light scattering [26] with frequency shifts in the scattered light. This process can also be seen as a random detuning of the optical cavity since it modifies its optical length $L^{(n)}_{\text{op}}$.

In the present case, we will be interested in the fraction of the scattering that is coupled to the cavity modes, with small shifts in the frequency (within the cavity bandwidth). The Hamiltonian which correctly models this type of photon-phonon interaction is known as the optomechanical Hamiltonian [27], which for this case is given by

$$\hat{H}_g = \sum_{n=0}^{2} \sum_{j=1}^{3} \hat{H}_g^{(n,j)}, \quad (33)$$

where

$$\hat{H}_g^{(n,j)} = -\hbar g_{nj} \hat{a}^{(n)\dagger}(t) \hat{a}^{(n)}(t) [\hat{d}^{(j)}(t) + \hat{d}^{(j)\dagger}(t)] \quad (34)$$

is the optomechanical Hamiltonian for the optical mode $\hat{a}^{(n)}$ coupled to the mechanical vibration mode $\hat{d}^{(j)}$. We may consider three possible modes of oscillation: one longitudinal, with propagation parallel to the wave vector of the field, and two transversal modes. The optomechanical coupling strength g_{nj} is expressed as a frequency. It quantifies the interaction between a single phonon and a single photon. The Hamiltonian in Eq. (34) reveals that the interaction of a vibrating nonlinear crystal with the radiation field is fundamentally a nonlinear process, involving three operators (three-wave mixing), coupling photon number operators to the creation and annihilation of phonons.

Following a procedure similar to that in Sec. II, we can write the bosonic operator $d^{(j)}$ with the help of the Fourier transform as

$$\hat{d}^{(j)}(t) = \int_0^\infty d\Omega_m e^{-i\Omega_m t} \hat{d}^{(j)}_{\Omega_m}, \quad (35)$$

with $\hat{d}^{(j)}_{\Omega_m}$ being the phonon annihilation operator in the mechanical mode of frequency Ω_m. The Hamiltonian in Eq. (33) can also be described by a sum of contributing terms over many

different frequencies as $\hat{H}_g = \int_\epsilon^\infty d\Omega \hat{H}_g(\Omega)$, where

$$\hat{H}_g(\Omega) = \sum_{n=0}^{2}\sum_{j=1}^{3} -\hbar g_{nj}\big[\alpha_{\omega_n}\big(\hat{a}^{(n)\dagger}_{\omega_n-\Omega}\hat{d}^{(j)\dagger}_{\Omega} + \hat{a}^{(n)\dagger}_{\omega_n+\Omega}\hat{d}^{(j)}_{\Omega}\big) + \text{H.c.}\big]. \tag{36}$$

Note that, satisfying energy conservation, different processes may occur from the annihilation of a photon of the carrier, described in the linearization by the field amplitude α_{ω_n}. We may have either the production of a photon in the lower sideband and the production of a phonon from the annihilation of a carrier photon or the production of a photon in the upper sideband with the annihilation of a phonon. The reverse processes are described by the Hermitian conjugate terms.

The complete Hamiltonian of the system, which includes the parametric down-conversion and the photon-phonon interaction, is given by

$$\hat{H}(\Omega) = \hat{H}_\chi(\Omega) + \hat{H}_g(\Omega), \tag{37}$$

where $\hat{H}_\chi(\Omega)$ and $\hat{H}_g(\Omega)$ are given by the Eqs. (3) and (36), respectively. Now a complete evaluation of the contributions of both parametric down-conversion and Brillouin scattering to the OPO dynamics can be performed.

B. Equations of motion for the field quadrature operators

The evolution of the system should now include the modes of the phonon bath. Let $\vec{\mathbb{A}} = (\vec{\mathbf{A}}, \vec{\mathbf{D}})^T$, where the field operator vector $\vec{\mathbf{A}}$ was defined in Sec. III and $\vec{\mathbf{D}} = (\hat{d}^{(1)}_\Omega \hat{d}^{(1)\dagger}_\Omega \hat{d}^{(2)}_\Omega \hat{d}^{(2)\dagger}_\Omega \hat{d}^{(3)}_\Omega \hat{d}^{(3)\dagger}_\Omega)^T$ lists the bosonic operators on the phononic reservoirs. Therefore, the set of differential equations describing the dynamics of the operators can be written in compact form as follows:

$$\frac{d\vec{\mathbb{A}}}{d\xi} = \mathbb{M}_{(\chi,g)}\vec{\mathbb{A}}, \tag{38}$$

where

$$\mathbb{M}_{(\chi,g)} = \begin{pmatrix} \mathbf{M}_\chi & i\mathbf{J}_g \\ i\mathbf{K}_g & \mathbf{0}_{6\times 6} \end{pmatrix}. \tag{39}$$

Here $\mathbf{M}_\chi = \mathbf{\Lambda}(\mathbf{M}_{\chi s} \oplus \mathbf{M}_{\chi a})\mathbf{\Lambda}^{-1}$, and

$$\mathbf{J}_g = \begin{pmatrix} \mathbf{L} \\ \mathbf{L}' \end{pmatrix}, \quad \mathbf{K}_g = (\mathbf{L}^\dagger \quad -\mathbf{L}'^\dagger), \tag{40}$$

where

$$\mathbf{L}_{nj} = g_{nj}\begin{pmatrix} \alpha_{\omega_n} & 0 \\ 0 & -\alpha^*_{\omega_n} \end{pmatrix}, \tag{41}$$

$$\mathbf{L}'_{nj} = g_{nj}\begin{pmatrix} 0 & \alpha_{\omega_n} \\ -\alpha^*_{\omega_n} & 0 \end{pmatrix} \tag{42}$$

are the element matrices of matrices $\mathbf{L}$ and $\mathbf{L}'$, respectively. In Eq. (40) the dagger denotes the conjugate transpose of the matrix.

The solution of Eq. (38) is given by

$$\vec{\mathbb{A}}|_{\xi=1} = \mathbb{G}(\chi,g)\vec{\mathbb{A}}|_{\xi=0}, \tag{43}$$

where

$$\mathbb{G}(\chi,g) = \exp\left(\int_0^1 d\xi\, \mathbb{M}_{(\chi,g)}\right). \tag{44}$$

C. Modeling the optical cavity

Following a procedure similar to that in Sec. IV, we get similar expressions for the output fields of the cavity. Specifically,

$$\vec{\mathbb{A}}_{\mathrm{R}} = \mathbb{R}_{(\chi,g)}\vec{\mathbb{A}}_{\mathrm{in}} + \mathbb{T}'_{(\chi,g)}\vec{\mathbb{A}}_\nu. \tag{45}$$

The expressions for the matrices $\mathbb{R}_{(\chi,g)}$ and $\mathbb{T}'_{(\chi,g)}$ are similar to those given in Eqs. (25) and (26) but with the following modifications to account for the phonon operators:

$$\begin{aligned} \boldsymbol{\varphi} &\to \Psi = (\boldsymbol{\varphi} \oplus \mathbf{0}_{6\times 6}), \\ \mathbf{R} &\to \mathbb{R} = (\mathbf{R} \oplus \mathbf{0}_{6\times 6}), \\ \mathbf{T} &\to \mathbb{T} = (\mathbf{T} \oplus \mathbf{1}_{6\times 6}), \\ \mathbf{R}' &\to \mathbb{R}' = (\mathbf{R}' \oplus \mathbf{0}_{6\times 6}), \\ \mathbf{T}' &\to \mathbb{T}' = (\mathbf{T}' \oplus \mathbf{1}_{6\times 6}). \end{aligned}$$

D. Solution for the Gaussian quantum state: Covariance matrix in the eigenbasis of quadrature operators

In analogy with Eq. (29), the covariance matrix for all fields (optical and phononic) is

$$\mathbb{V}_{\mathrm{R}} = \widetilde{\mathbb{R}}_{(\chi,g)}\mathbb{V}_{\mathrm{in}}\widetilde{\mathbb{R}}^T_{(\chi,g)} + \widetilde{\mathbb{T}}'_{(\chi,g)}\mathbb{V}_\nu\widetilde{\mathbb{T}}'^T_{(\chi,g)}. \tag{46}$$

Considering the case where field inputs are in the vacuum state and the phonon reservoir is in a thermal state, $\mathbf{V}_{\mathrm{th}} = (1+2\bar{n}_{\mathrm{th}})\mathbf{1}_{6\times 6}$, we have

$$\mathbb{V}_{\mathrm{in}} = \mathbb{V}_\nu = (\mathbf{1}_{12\times 12} \oplus \mathbf{V}_{\mathrm{th}}), \tag{47}$$

considering here that the three phonon modes of the reservoir have the same temperature and the same average number of phonons $\bar{n}_{\mathrm{th}}$.

The resulting covariance matrix is given by

$$\mathbf{V}_s = \begin{pmatrix} \rho^{(0)} & e_1 & \mu^{(01)} & e_2 & \mu^{(02)} & e_3 \\ e_1 & \beta^{(0)} & e_4 & \nu^{(01)} & e_5 & \nu^{(02)} \\ \mu^{(01)} & e_4 & \rho^{(1)} & e_6 & \zeta^{(12)} & e_7 \\ e_2 & \nu^{(01)} & e_6 & \beta^{(1)} & e_8 & \epsilon^{(12)} \\ \mu^{(02)} & e_5 & \zeta^{(12)} & e_8 & \rho^{(2)} & e_9 \\ e_3 & \nu^{(02)} & e_7 & \epsilon^{(12)} & e_9 & \beta^{(2)} \end{pmatrix}, \tag{48}$$

and

$$\mathbf{C}_{s/a} = \begin{pmatrix} \delta^{(0)} & 0 & h_1 & -\kappa^{(01)} & h_2 & -\kappa^{(02)} \\ 0 & \delta^{(0)} & \lambda^{(01)} & h_3 & \lambda^{(02)} & h_4 \\ h_3 & \kappa^{(01)} & \delta^{(1)} & 0 & h_5 & -\varrho^{(12)} \\ -\lambda^{(01)} & h_1 & 0 & \delta^{(1)} & \eta^{(12)} & h_6 \\ h_4 & \kappa^{(02)} & h_6 & \varrho^{(12)} & \delta^{(2)} & 0 \\ -\lambda^{(02)} & h_2 & -\eta^{(12)} & h_5 & 0 & \delta^{(2)} \end{pmatrix}. \tag{49}$$

A direct comparison with the matrices in Eqs. (31) and (32) shows many additional features coming from this added

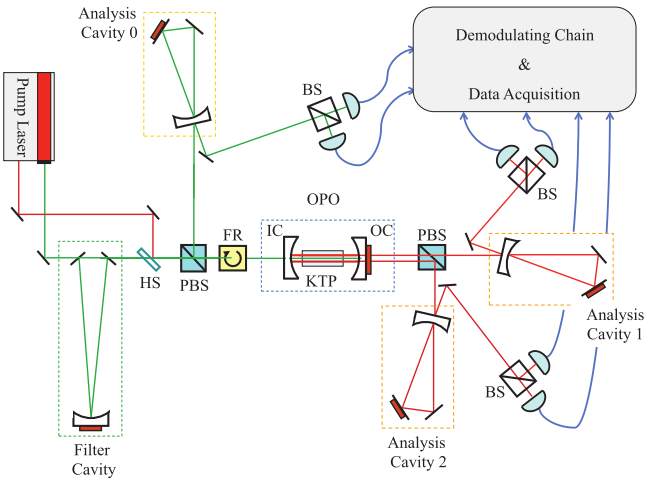

FIG. 2. Setup for the reconstruction of the OPO beams' covariance matrix. PBS, polarizing beam splitter; BS, 50:50 beam splitter; HS, harmonic separator; IC, input coupler; OC, output coupler (OPO cavity); FR, Faraday rotator.

thermal reservoir. It is curious that even in the absence of phonons in the reservoir, those terms still appear due to the photon-phonon coupling of the zero-temperature fluctuations. Nevertheless, these terms are small in this case and will not significantly affect the covariance, even though the resulting state of the field is no longer pure due to the coupling to extra modes from the crystal.

VII. EXPERIMENTAL RESULTS

The model developed here can be directly compared to the experimental results obtained from the setup described in [18]. The system is a triply resonant OPO operating above threshold, and the experimental setup is depicted in Fig. 2. The OPO cavity is pumped by the second harmonic of a doubled Nd:YAG laser, filtered with a mode-cleaning cavity to ensure that pump fluctuations are reduced to the standard quantum level in amplitude and phase for frequencies above 20 MHz.

The filtered pump beam is then injected in the OPO, with adjustable power, through the input coupler (IC) with a reflectivity of 70% for the pump field (532 nm) and high reflectivity (>99%) at 1064 nm. The reflected pumped field is recovered from the Faraday rotator (FR). The infrared output coupler (OC) has a reflectivity of 96% at ≈1064 nm and high reflectivity (>99%) at 532 nm. Both mirrors are deposited on concave substrates with a curvature radius of 50 mm. The crystal is a type-II phase-matched KTP (potassium titanyl phosphate, $KTiOPO_4$) with length $l = 12$ mm, average refractive index $n = 1.81(1)$, and antireflective coatings for both wavelengths. The average free spectral range for the three modes is found to be 4.3(5) GHz. The cavity finesse is 15 for the pump mode and 124 for the signal and idler modes (the latter is defined as the mode with the same polarization as the pump). The overall detection efficiencies are 87% for the infrared beams and 65% for the pump, accounting for detector efficiencies and losses in the beam paths. The threshold power is 60 mW, and the maximum pump power was 75% above the threshold. In order to reduce the effect of phonon noise on the system, the crystal is cooled to 260 K, and the OPO is kept in a vacuum chamber to avoid condensation.

Phase noise measurements were performed using the ellipse rotation method described in [28,29], with the help of analysis cavities. Cavities 1 and 2 (for the transmitted infrared beams) have bandwidths of 14(1) MHz, and cavity 0 (for the reflected pump) has a bandwidth of 12(1) MHz. This ensures a full rotation of the noise ellipse for the chosen analysis frequency of 21 MHz. Mode matching of the beams to the analysis cavities was better than 95%. Combining in-quadrature electronic local oscillators and cavity detection [18,19], we were able to reconstruct the covariance matrix of the output sidebands. Since the detected modes are of Gaussian nature [30], determination of the covariance matrix is equivalent to the complete tomography of the output state of the sidebands of the intense optical fields involved.

Covariances for the intensity fluctuations are shown in Fig. 3 in terms of the symmetric and antisymmetric modes, which results in a compact presentation of the covariance matrix. They present good agreement of the theory and the experiment. Deviations for the pump field at higher pump power are consistent with the effects of mismatch in the pumping field, which are aggravated by thermal lensing of the crystal. The pump cavity mode will be more depleted with growing pump power, and the contributions of unmatched modes will be more relevant, degrading the measurement of the variance and contributing as an effective loss in detection. Nevertheless, correlations are less affected in this case and present better agreement. It is curious to notice that correlations between the symmetric and antisymmetric modes are observed for pump and signal (or idler) correlations, as predicted in [18], revealing that there is more information on the system beyond the three-mode description. A full description of the measured state should necessarily involve six fields, and the distinct role of each sideband becomes relevant for the tomography of the system.

Phase quadrature measurements of fields of distinct colors are possible through the use of analysis cavities. The results shown in Fig. 4 were evaluated with a limited number of adjusting variables to describe the phonon coupling. The complete model involves three coupling channels between each mode of the carrier and distinct reservoirs, one for each oscillating mode of a crystal. Nevertheless, a toy model considering that pump and idler are coupled to the same reservoir (since they have the same polarization) and the orthogonally polarized signal with additional coupling to a second reservoir can be used to adjust the curves to the data. The best results were obtained with $g_{01} = 8.0\times10^{-3}$ for the pump coupling, $g_{21} = 3.6\times10^{-3}$ for the idler coupling, and $g_{11} = 1.9\times10^{-3}$ for signal coupling to one of the reservoirs and $g_{12} = 2.7\times10^{-3}$ for signal coupling to the second reservoir. Thermal phonon population density was arbitrarily set to $N_{th} = 100$, acting just as a multiplicative constant in our model at high temperatures. It is curious to notice that $\sqrt{g_{11}^2 + g_{12}^2} \sim g_{21}$ and $g_{01} \sim 2g_{21}$, consistent with the scaling with wavelength described in the semiclassical model for the phonon noise [25].

It is clear that the photon-phonon coupling leads to an additional noise in the system, which should degrade purity. This excess noise can be observed in Fig. 4, where the solid lines present the expected results with phonon noise, and the

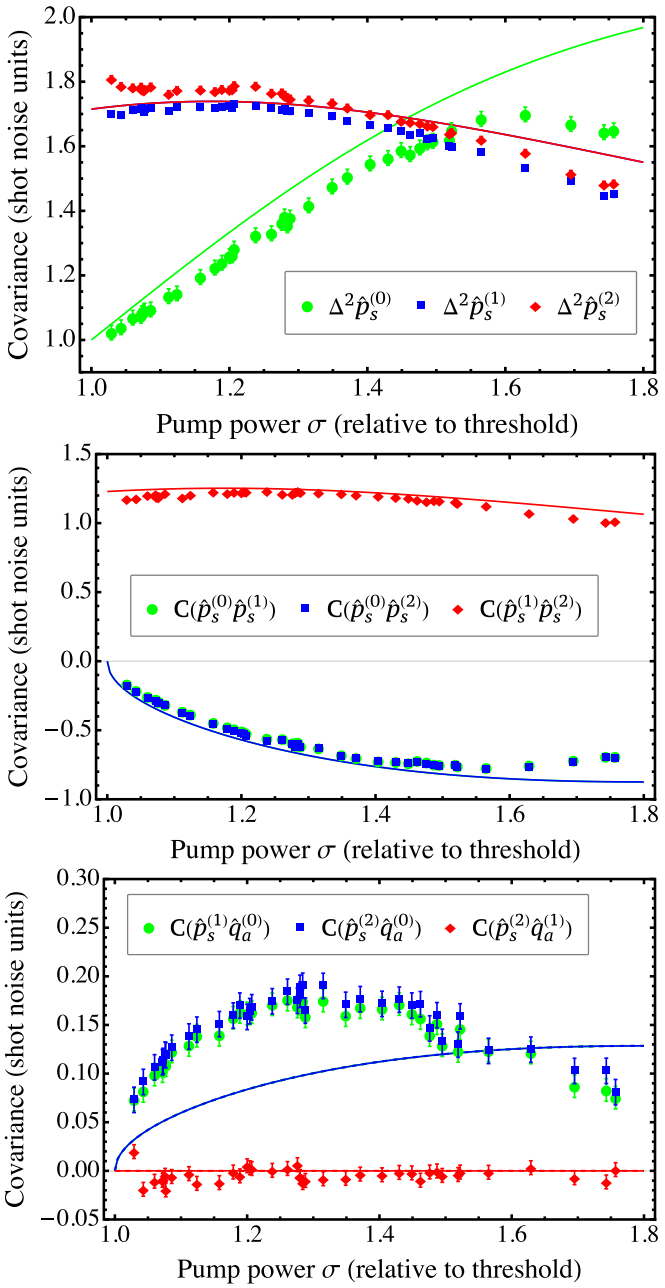

FIG. 3. Measured variances of the amplitudes of the three fields coming from the OPO, in the symmetric description, followed by their respective correlations. Cross correlations between symmetric and antisymmetric modes.

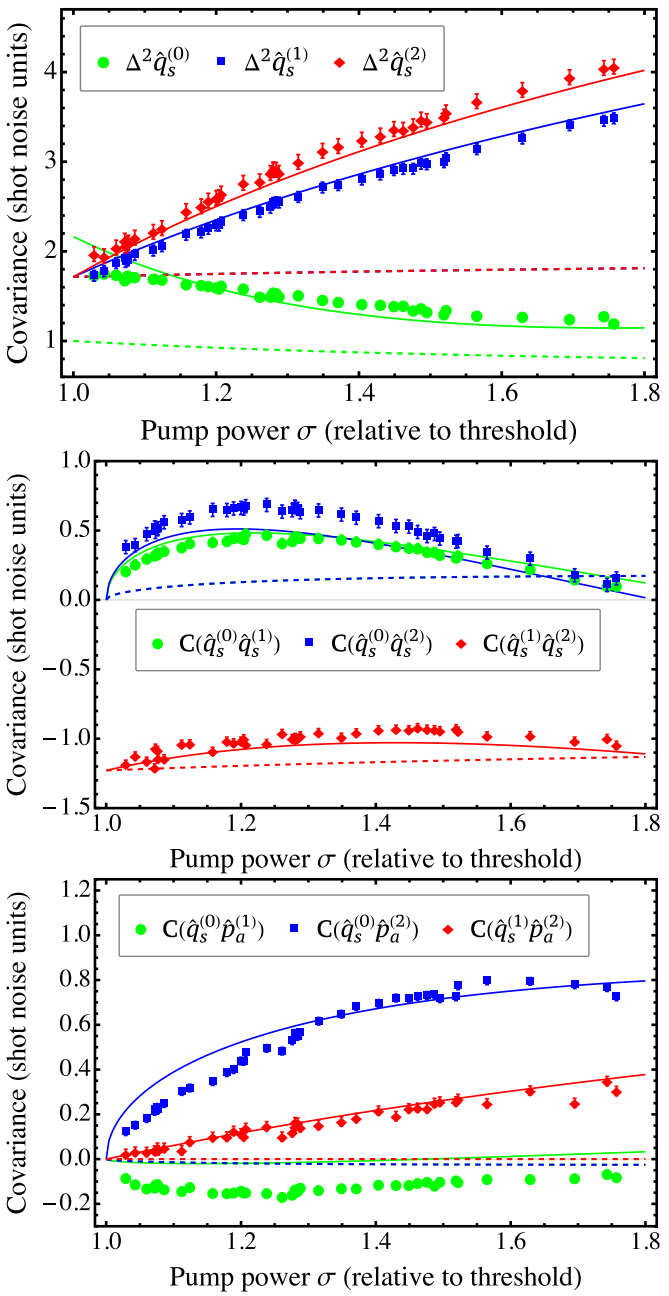

FIG. 4. Measured variances of the phase of the three fields coming from the OPO, in the symmetric description, followed by their respective correlations. Cross correlations between symmetric and antisymmetric modes. Dashed lines are the result we would expect in the absence of phonon noise.

dashed lines present the corresponding values in the absence of this noise source. This coupling prevents the observation of phase squeezing of the pump mode in the present condition and adds noise to signal and idler fields. Since this additional noise is not perfectly correlated, it will lead to degradation of the squeezing level at the sum of the phases, as we would expect in the generation of entangled modes of the field [17]. Nevertheless, quantum correlations for two [5] and three modes [7] can be observed if adequate control of the phonons is available from the cooling of the crystal.

So far, we have presented all the measurements for the 18 terms in matrices given in Eqs. (48) and (49). Nevertheless, a complete description of the system should involve all the correlations between the phase and amplitudes of each field in the symmetric and antisymmetric descriptions. The present model shows that for perfect resonance of the carriers the contribution of these terms should be zero. Experimental results are close to this situation for low pump powers, as can be seen in Fig. 5. Cross correlations become effectively nonzero for growing pump powers, where thermal effects should provide some change in the refractive index, leading to small detunings of the carrier modes.

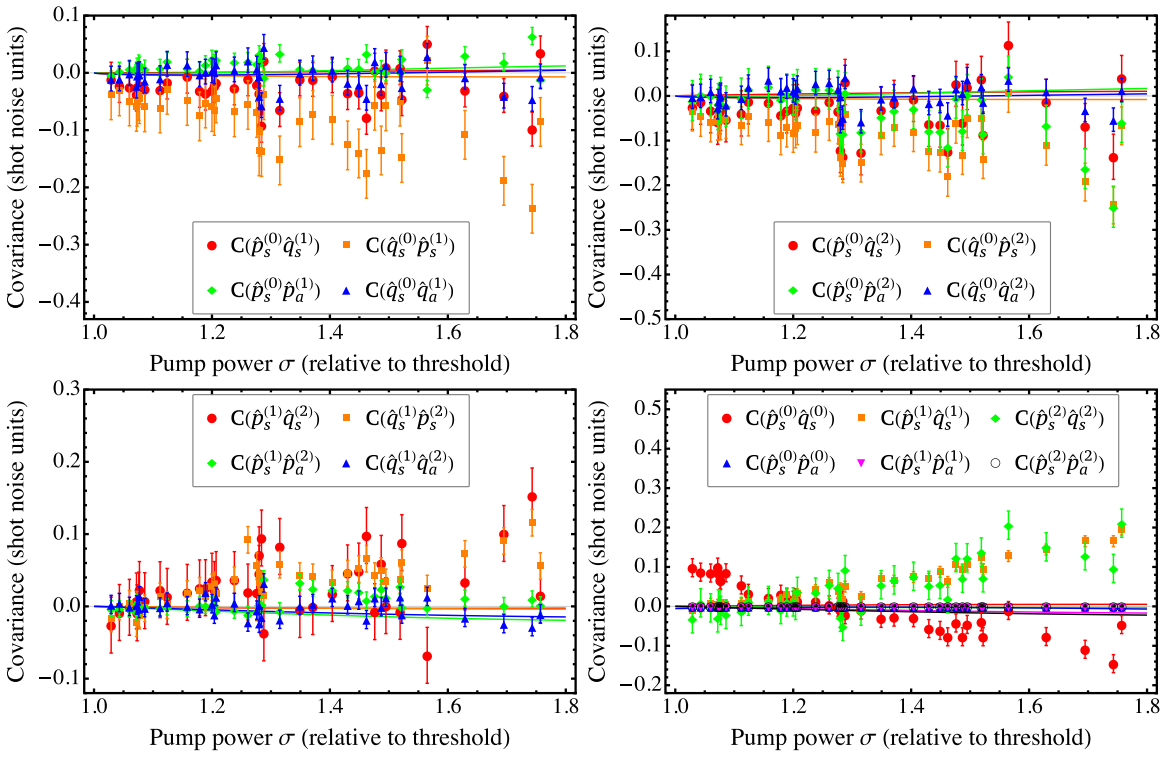

FIG. 5. Measured correlations between amplitude and phase for each mode in symmetric and antisymmetric descriptions.

VIII. CONCLUSION

In the continuous-variable domain, the combined use of self-homodyning [31] and demodulation by in-quadrature local oscillators [18] allows the complete reconstruction of the state of six modes of the field in an above-threshold OPO. These modes are related to the sidebands of the down-converted fields, generated by the nonlinear process, and the pump field, reflected by the cavity. The results we obtained are in good agreement with the detailed model developed here, involving the transformation of the field operators in their reflection by a cavity, the nonlinear coupling among the fields by the crystal, and the photon-phonon coupling. For the linear approach we chose, the model reproduces the so-called semiclassical model of the OPO, where quantized fields can be associated with stochastic fluctuations in a Langevin equation, leading to a spectral matrix, associated with the Fourier transform of the two-time correlation of the output fields. In the present case, discrepancies between our model and the semiclassical one are smaller than 4% of the standard quantum level (except for amplitude variance of the pump, reaching 9%), with both being compatible with the experimental results.

The main result of the developed model is the demonstration that the imaginary part of the spectral matrix, i.e., the correlations between symmetric and asymmetric combinations of sidebands [18], has its physical origin not in the nonlinear process but in the evolution of the fields inside the cavity, combined with the effective beam-splitter transformation for down-converted and pump modes, explicitly derived in the linearized model. This particular effect is not explicit in the semiclassical treatment. The asymmetries in phase evolution of upper and lower sidebands lead to the coupling of their symmetric and asymmetric combinations. These effects will be small for reduced analysis frequencies and will be maximized as they get closer to the OPO cavity bandwidth.

The presented model was shown to be suitable for the reconstruction of the covariance matrix in a linearized regime, which is valid for small intracavity gain. Since the output fields are in a Gaussian state for all practical purposes [30], it characterizes a complete state tomography involving six modes of an OPO in a wide range of pump values, opening the path to explore the structure of hexapartite entanglement in this system [20].

ACKNOWLEDGMENTS

The authors acknowledge the support from Grant No. 2010/08448-2, Fundação de Amparo à Pesquisa do Estado de São Paulo (FAPESP), Conselho Nacional de Desenvolvimento Científico e Tecnológico, and Coordenação de Aperfeiçoamento de Pessoal de Nível Superior.

[1] L. A. Wu, H. J. Kimble, J. L. Hall, and H. F. Wu, Phys. Rev. Lett. **57**, 2520 (1986).

[2] A. Heidmann, R. J. Horowicz, S. Reynaud, E. Giacobino, C. Fabre, and G. Camy, Phys. Rev. Lett. **59**, 2555 (1987).

[3] Z. Y. Ou, S. F. Pereira, H. J. Kimble, and K. C. Peng, Phys. Rev. Lett. **68**, 3663 (1992).

[4] K. Kasai, Gao Jiangrui, and C. Fabre, Europhys. Lett. **40**, 25 (1997); K. S. Zhang, T. Coudreau, M. Martinelli, A. Maître, and C. Fabre, Phys. Rev. A **64**, 033815 (2001).

[5] A. S. Villar, L. S. Cruz, K. N. Cassemiro, M. Martinelli, and P. Nussenzveig, Phys. Rev. Lett. **95**, 243603 (2005).
[6] K. N. Cassemiro, A. S. Villar, M. Martinelli, and P. Nussenzveig, Opt. Express **15**, 18236 (2007).
[7] A. S. Coelho, F. A. S. Barbosa, K. N. Cassemiro, A. S. Villar, M. Martinelli, and P. Nussenzveig, Science **326**, 823 (2009).
[8] C. M. Caves, Phys. Rev. D **23**, 1693 (1981).
[9] The LIGO Scientific Collaboration, Nat. Phys. **7**, 962 (2011).
[10] A. Furusawa, J. L. Sørensen, S. L. Braunstein, C. A. Fuchs, H. J. Kimble, and E. S. Polzik, Science **282**, 706 (1998).
[11] S. Takeda, T. Mizuta, M. Fuwa, P. van Loock, and A. Furusawa, Nature (London) **500**, 315 (2013).
[12] N. C. Menicucci, P. van Loock, M. Gu, C. Weedbrook, T. C. Ralph, and M. A. Nielsen, Phys. Rev. Lett. **97**, 110501 (2006).
[13] S. Yokoyama, R. Ukai, S. C. Armstrong, C. Sornphiphatphong, T. Kaji, S. Suzuki, J. Yoshikawa, H. Yonezawa, N. C. Menicucci, and A. Furusawa, Nat. Photon. **7**, 982 (2013).
[14] O. Pinel, P. Jian, R. M. de Araújo, J. Feng, B. Chalopin, C. Fabre, and N. Treps, Phys. Rev. Lett. **108**, 083601 (2012).
[15] M. Chen, N. C. Menicucci, and O. Pfister, Phys. Rev. Lett. **112**, 120505 (2014).
[16] H. Wang, C. Fabre, and J. Jing, Phys. Rev. A **95**, 051802 (2017).
[17] M. D. Reid and P. D. Drummond, Phys. Rev. Lett. **60**, 2731 (1988); Phys. Rev. A **40**, 4493 (1989).
[18] F. A. S. Barbosa, A. S. Coelho, K. N. Cassemiro, P. Nussenzveig, C. Fabre, A. S. Villar, and M. Martinelli, Phys. Rev. A **88**, 052113 (2013).
[19] F. A. S. Barbosa, A. S. Coelho, K. N. Cassemiro, P. Nussenzveig, C. Fabre, M. Martinelli, and A. S. Villar, Phys. Rev. Lett. **111**, 200402 (2013).
[20] F. A. S. Barbosa, A. S. Coelho, L. F. Muñoz-Martínez, L. Ortiz-Gutiérrez, A. S. Villar, P. Nussenzveig, and M. Martinelli, Phys. Rev. Lett. **121**, 073601 (2018).
[21] D. F. Walls and G. J. Milburn, *Quantum Optics* (Springer, New York, 2008).
[22] A. S. Villar, M. Martinelli, C. Fabre, and P. Nussenzveig, Phys. Rev. Lett. **97**, 140504 (2006).
[23] T. Debuisschert, A. Sizmann, E. Giacobino, and C. Fabre, J. Opt. Soc. Am. B **10**, 1668 (1993).
[24] M. J. Collett and C. W. Gardiner, Phys. Rev. A **30**, 1386 (1984).
[25] J. E. S. César, A. S. Coelho, K. N. Cassemiro, A. S. Villar, M. Lassen, P. Nussenzveig, and M. Martinelli, Phys. Rev. A **79**, 063816 (2009).
[26] R. W. Boyd, *Nonlinear Optics* (Academic Press, San Diego, 1992).
[27] C. K. Law, Phys. Rev. A **51**, 2537 (1995)
[28] P. Galatola, L. Lugiato, M. Porreca, P. Tombesi, and G. Leuchs, Opt. Commun. **85**, 95 (1991).
[29] A. S. Villar, Am. J. Phys. **76**, 922 (2008).
[30] A. S. Coelho, F. A. S. Barbosa, K. N. Cassemiro, M. Martinelli, A. S. Villar, and P. Nussenzveig, Phys. Rev. A **92**, 012110 (2015).
[31] A. Villar, M. Martinelli, and P. Nussenzveig, Opt. Commun. **242**, 551 (2004).